JOURNAL OF MATERIALS SCIENCE 32 (1997) 1815–1824

Micropyretic synthesis of Ni–Al intermetallic composites

HAO ZHANG, J. A. SEKHAR
Department of Materials Science and Engineering, International Center for Micropyretics, University of Cincinnati, Cincinnati, OH 45221, USA

Ni_3Al and NiAl intermetallic compounds and their composites are potential structural materials for high-temperature applications. Among the composites with different types of reinforcements, particulate-reinforced composites possess several advantages, such as isotropic properties, lower costs of reinforcement and easy fabrication. Particulate-reinforced composites also allow for a wider range of component geometry. In this article, Ni–Al–Cu composites with CeO_2 particulates were prepared using the micropyretic synthesis techniques. The effect of chemical composition on the processing response parameters, the phases of products, the microstructure and mechanical properties of the composites were studied. X-ray diffraction results indicated that the phases of the synthesized composites were critically dependent upon the aluminium content. The final porosity of the composites decreased with an increase in the aluminium content. The flexural bending test showed a variation in the flexural strength of the composites with changing microstructure. The flexural strength and the elastic modulus increased with the aluminium content and the final density.

1. Introduction

Ni_3Al and NiAl intermetallic compounds and their composites are potential structural materials for high-temperature applications [1–6]. Amongst composites with different types of reinforcements, particulate-reinforced composites possess several advantages, such as a variety of isotropic properties, lower costs of reinforcement and fabrication. Particulate-reinforced composites also allow for a wider range of fabrication processes and component geometry [7]. Micropyretic synthesis has been used to synthesize intermetallics and their composites, ceramics and their composites and refractory compounds [9–13]. Several workers have studied micropyretic synthesis of nickel aluminides and their composites [9–12, 14–22]. In these studies, elemental nickel and aluminium powders with the desired stoichiometric compositions were mixed, compacted and reacted to produce Ni_3Al, NiAl intermetallics and their composites. These studies have shown interesting processing behaviour and mechanical properties of Ni_3Al, NiAl intermetallics and their composites. Recently, CeO_2 coated Ni_3Al–Cu intermetallic alloy composites containing CeO_2 particles have been developed as potential nonconsumable anode substrates for aluminium electrowinning in the Hall–Heroult cells [23]. The CeO_2-coated Ni_3Al–Cu–CeO_2 composite anode substrates have shown good performances in the Hall–Heroult cell tests due to their excellent oxidation resistance and the protection provided by the CeO_2 coating.

In the present study, several reactive synthesized intermetallic composites based on Ni_3Al–Cu and NiAl–Cu with CeO_2 particles were studied. The effect of processing parameters, such as chemical composition, nickel particle size, and heating rate, on the response processing parameters, microstructure and mechanical properties, were studied.

2. Experimental procedure

The materials studied in this work were Ni–Al–Cu–CeO_2 composites with the aluminium content ranging from 4–28 wt %. The chemical composition of the composites is listed in Table I. Fig. 1 shows the liquidus surface in the Ni–Al–Cu ternary phase diagram.

2.1. Processing

Compositions of nickel, aluminium, copper and CeO_2 powders in different ratios were weighed and mixed in a plastic jar. The aluminium, copper, CeO_2 powders and three different types of nickel powders were used in this study. The characteristics of the powders are described in detail in Table II. The mixed powder was pressed into two differently shaped specimens for different property measurements. The first specimen was pressed in a cylindrical die, with dimensions of 2.54 cm diameter and about 1–2 cm high, in a uniaxial single-acting press. The second specimen was pressed in a rectangular die with dimensions of 5.08 cm × 1.27 cm × ~ 0.635 cm (2 in × 0.5 in × ~ 0.25 in) according to ASTM B312. The compaction pressure used was from 108–260 MPa.

TABLE I Chemical composition of Ni–Al–Cu–CeO_2 composites studied in this work (wt %)

Sample	Al	Ni	Cu	CeO_2
A-1	4	84	10	2
A-2	6	82	10	2
A-3	8	80	10	2
A-4	10	78	10	2
A-5	12	76	10	2
A-6	16	72	10	2
A-7	20	68	10	2
A-8	28	60	10	2

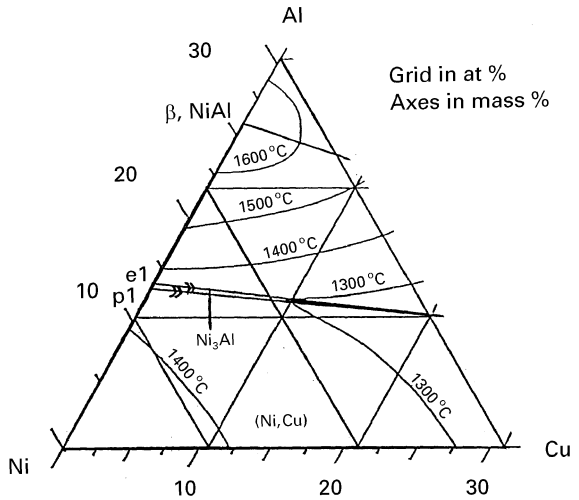

Figure 1 Liquidus surface at the nickel-rich corner in the Ni–Al–Cu ternary phase diagram [24].

TABLE II Characteristics of the different powders employed in this study

Powders	Vendor	Sieve size	Size (μm)	Purity (wt %)
Al	Johnson-Matthey	− 325	< 44	99.5
Ni(1)	Johnson-Matthey	− 100	< 149	99.5
Ni(2)	Johnson-Matthey	− 300	< 50	99.9
Ni(3)	Johnson-Matthey	–	~ 3	99.7
Cu	Aldrich	–	5–10	99
CeO_2	Johnson-Matthey	–	< 2	99.5

The green densities of the compacted specimens were determined from the weight and geometric measurements and were between about 50% and 70% of the theoretical density. The thermal explosion mode [9, 10, 13] was used to synthesize the compacted samples by heating the specimens in a furnace set at 600 and 800 °C until the reaction initiated over the whole specimens simultaneously. The combustion temperature, T_c, ignition temperature, T_i, and temperature profiles during synthesis, were measured using very fine W26%Re–W5%Re thermocouples (W26%Re and W5%Re wires were 0.127 cm diameter) firmly embedded in a small hole in the samples. The temperature profiles were recorded by connection to a data acquisition system and a computer.

2.2. Characterization

After micropyretic synthesis, the specimens were sectioned, ground and polished for further microstructural study and analysis. An ultrasonic cleaner was used to wash the specimens after grinding and polishing. Kalling's reagent, 5 g $CuCl_2$ + 100 ml HCl + 100 ml ethanol, was used to etch the specimens. The microstructure of the composites were observed using optical microscopy and scanning electron microscopy (SEM). The phases of the composites were identified by X-ray diffraction obtained in a Siemens D-500 diffractometer with CuK_α radiation (wavelength = 0.1540 051 nm) operating at 40 kV and 30 mA. The scanning step of 0.05° s^{-1} and the time constant of 1 s were used as the parameter of measurement in this work. The micrographs of the specimens were scanned in an optical scanner and then transmitted into a computer. The image analysis was used to measure and analyse the initial and final porosity of the composites. Mechanical tests, such as hardness and bending tests, were conducted on the composites synthesized by Ni(1) powder. A four-point bending test was performed in Instron 4206 universal test instruments. The tests were conducted following the ASTM B312 standard. The crosshead speed (deflection rate) of 0.25 in min^{-1} (~0.9 mm min^{-1}) was used for the bending tests.

3. Results and discussion

3.1. Green density of powder compacts

Table III gives the green density of the cylindrical compacted specimens with different compositions, compaction pressures and nickel particle sizes. Coarser nickel particles result in a higher green

TABLE III Green density of the powder compacts with different composition, nickel particle sizes, *d*, and compaction pressures

Sample no.	Al content (wt %)	Green density (g cm^{-3})								
		$d < 149$ μm			$d < 50$ μm			$d < 3$ μm		
		108 MPa (12.8×10^3 p.s.i.)	215 MPa (25.5×10^3 p.s.i.)	260 MPa (38.3×10^3 p.s.i.)	108 MPa (12.8×10^3 p.s.i.)	215 MPa (25.5×10^3 p.s.i.)	260 MPa (38.3×10^3 p.s.i.)	108 MPa (12.8×10^3 p.s.i.)	215 MPa (25.5×10^3 p.s.i.)	260 MPa (38.3×10^3 p.s.i.)
A-1	4	5.74	6.42	6.82	5.21	5.68	6.20	4.24	4.91	5.36
A-3	8	5.52	6.07	6.43	5.03	5.43	6.00	4.03	4.69	5.14
A-5	12	5.23	5.81	6.13	4.83	5.29	5.68	3.81	4.51	4.96
A-6	16	4.97	5.42	5.90	4.60	5.04	5.49	3.69	4.27	4.74
A-7	20	4.68	5.13	5.48	4.34	4.76	5.21	3.55	3.96	4.62
A-8	28	4.17	4.50	5.00	3.91	4.27	4.67	3.31	3.59	4.30

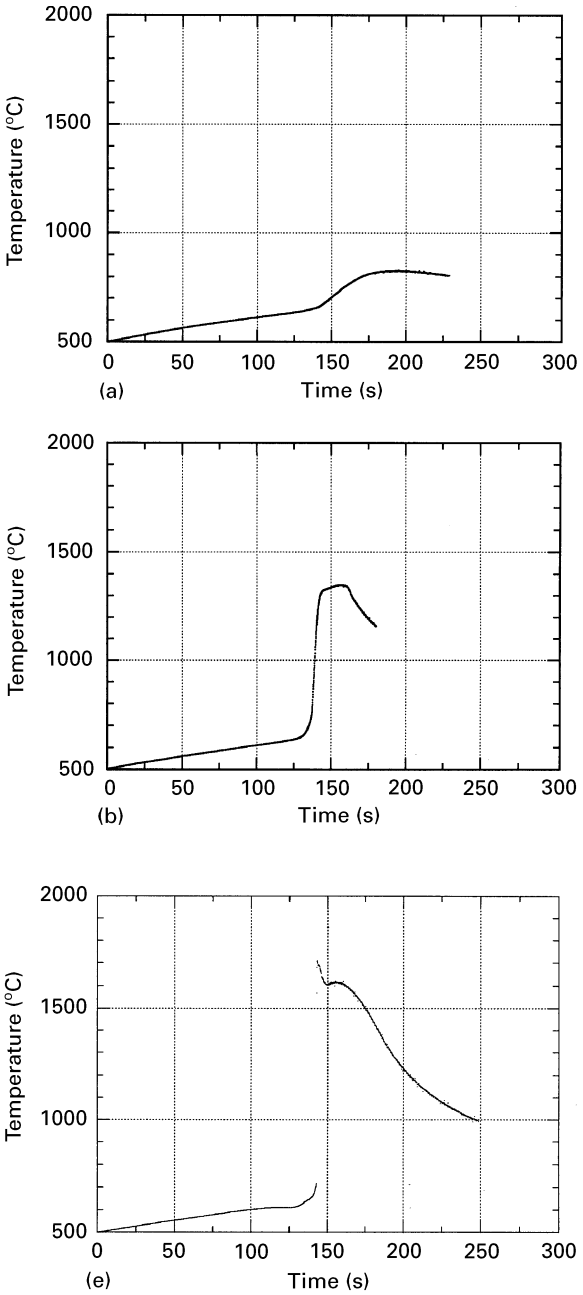

Figure 2 Temperature profiles during micropyretic synthesis of Ni–Al–10Cu–2CeO_2 composites: (a) 4 wt % Al, (b) 8 wt % Al, (c) 12 wt % Al (d) 16 wt % Al, (e) 28 wt % Al (nickel powder size − 100 mesh, compaction pressure 215 MPa, furnace temperature 600 °C.)

TABLE IV Measured T_i and T_c for the synthesis of Ni–Al–10Cu– 2CeO_2 composites

	Sample				
	A-1	A-3	A-5	A-6	A-8
Al (wt %)	4	8	12	16	28
T_i (°C)	645	650	640	640	640
T_c (°C)	825	1320	1345	1410	1715

density. The green density decreased with increasing aluminium content, and increased with an increase in compaction pressure.

3.2. Micropyretic synthesis

The ignition temperature, T_i, and combustion temperature, T_c, are the important response processing parameters which are dependent on some of the initial processing parameters. A knowledge of T_i, T_c and the temperature profile during the synthesis, provides important information on the heating rate of the specimens, the states of each compositional element, and the cooling rate of the specimens following the synthesis.

3.2.1. Effect of aluminium content

Fig. 2 shows the typical temperature profiles during the micropyretic synthesis of Ni–Al–10Cu–2CeO_2 composites containing aluminium from 4–28 wt %. The synthesis was performed by the thermal explosion mode in a furnace set at 600 °C, which produced the equivalent heating rate of 1.2 °C s^{-1} before the synthesis occurred. Table IV gives the measured T_i and T_c obtained from Fig. 2.

For the specimen containing 4 wt %Al, Fig. 2a, the temperature profile increases slowly with a small slope after it reaches T_i, then reaches the maximum temperature, T_c. In Fig. 2b and c, the temperature profiles show an abrupt increase in temperature from T_i to T_c in a very short time. The temperature "plateaus" appear in both these profiles where the temperature is kept unchanged for a while after reaching T_c. The "plateau" in the temperature profile indicates that micropyretic synthesis of these two compositions involves a liquid to solid phase transformation which corresponds to a release in latent heat at T_c. In Fig. 2c,

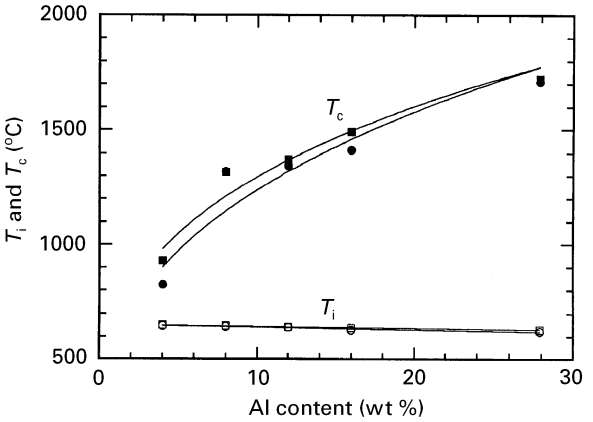

Figure 3 Dependence of (○, □) T_i and (●, ■) T_c on aluminium content and heating rate (or furnace temperature). Nickel powder size − 300 mesh, compaction pressure 215 MPa. (○, ●) 600 °C, (□, ■) 800 °C.

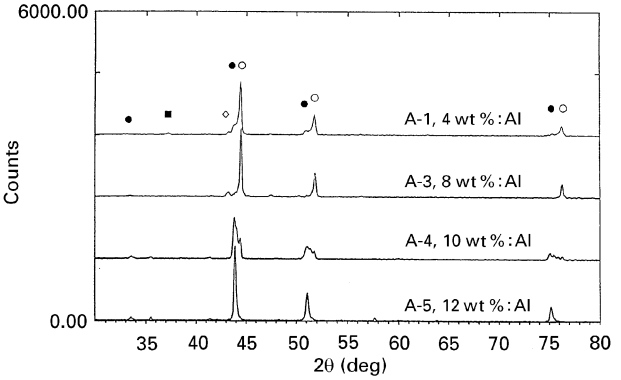

Figure 4 X-ray diffraction spectra of the Ni–Al–10Cu–2CeO_2 composites, containing 4–12 wt % Al. (○) Ni, (◇) Cu, (■) NiO, (●) Ni_3Al, (◇) CeO_2.

the "plateau" lasts about 45 s. The difference in duration of the "plateaus" in Fig. 2b and c may be associated with the amount of liquid phase formed during the synthesis.

Temperature peaks and the subsequents "plateaus" appear in Fig. 2d and e, in which the measured T_c values are 1410 and 1715 °C, respectively. The measured temperatures at the "plateaus" are 1370 and 1630 °C, respectively. Because T_c in Fig. 2e is higher than the melting points of Ni, Ni_3Al(Cu) and NiAl(Cu), the liquid–liquid state reactions take place in the synthesis of sample A-8. The solidification of the liquid products causes the "plateaus" in the temperature profiles. Fig. 3 shows the dependence of T_i and T_c on aluminium content in Ni–Al–10Cu–2CeO_2. As shown in Fig. 2, T_c increases with increasing aluminium content, from 840 to 1720 °C. However, T_i decreases slightly with aluminium content, ranging from 620–650 °C.

The temperature measurement shows that the synthesis reactions can occur at a furnace temperature of 600 °C, which is lower than the melting point of aluminium (660 °C). This indicates that the solid–solid state reactions between nickel and aluminium particles occur prior to the reactants reacting completely when the temperature of the specimens is raised from room temperature to T_c. In addition, the oxidation of the aluminium powder to form Al_2O_3 during heating also helps the reaction to occur.

3.2.2. Effect of heating rate

In this study, different heating rates were achieved by reacting the powder compacts in a furnace set at different temperatures. Two furnace temperatures, 600 and 800 °C, were used in these experiments. For the cylindrical compacts, the furnace temperatures of 600 and 800 °C produced the heating rates of 1.2 and 2.5 °C s^{-1}, respectively. Fig. 3 shows the dependence of T_i and T_c on aluminium content and heating rate. As can be seen in Fig. 3, T_c increases with aluminium content and heating rate. However, T_i decreases slightly with aluminium content, but does not change much with the heating rate. Philpot *et al.* [15] have reported that the heating rate influences the major combustion reaction in the case of the synthesis of nickel aluminide. Because the heating rate directly affects the extent of the formation of pre-combustion phases, it is expected that the heating rate will play an important role in the synthesis process [15]. As in the synthesis of Ni–Al, the synthesis of Ni–Al–Cu–CeO_2 composites also involves two reaction steps, i.e. pre-combustion and combustion reactions. Any factor influencing these two reactions will affect the whole reaction process, which determines T_c, the amount and the distribution of liquid phases, and hence will affect the microstructure of the composites.

3.3. Microstructure

3.3.1. X-ray diffraction

The phases in the synthesized composites were determined by X-ray diffraction. The results show that the phases are highly dependent on the aluminium content. However, the other processing parameters such as heating rate, nickel particle size and compaction pressure did not apparently influence the final phases of the composites. Fig. 4 shows the X-ray diffraction spectra of the composites in the Ni + Ni_3Al phase region. Table V gives the phases identified by X-ray diffraction. For the Ni_3Al and NiAl stoichiometric

TABLE V Phases identified in Ni–Al–10Cu–2CeO_2 composites by X-ray diffraction

	Sample				
	A-1	A-3	A-5	A-6	A-8
Al content (wt %)	4	8	12	16	28
Ni content (wt %)	84	80	76	72	60
Ni, Ni_3Al phases	Ni, Ni_3Al	Ni_3Al, Ni	Ni_3Al	Ni_3Al, NiAl	NiAl
Other phases	Cu, NiO	Cu	–	–	–

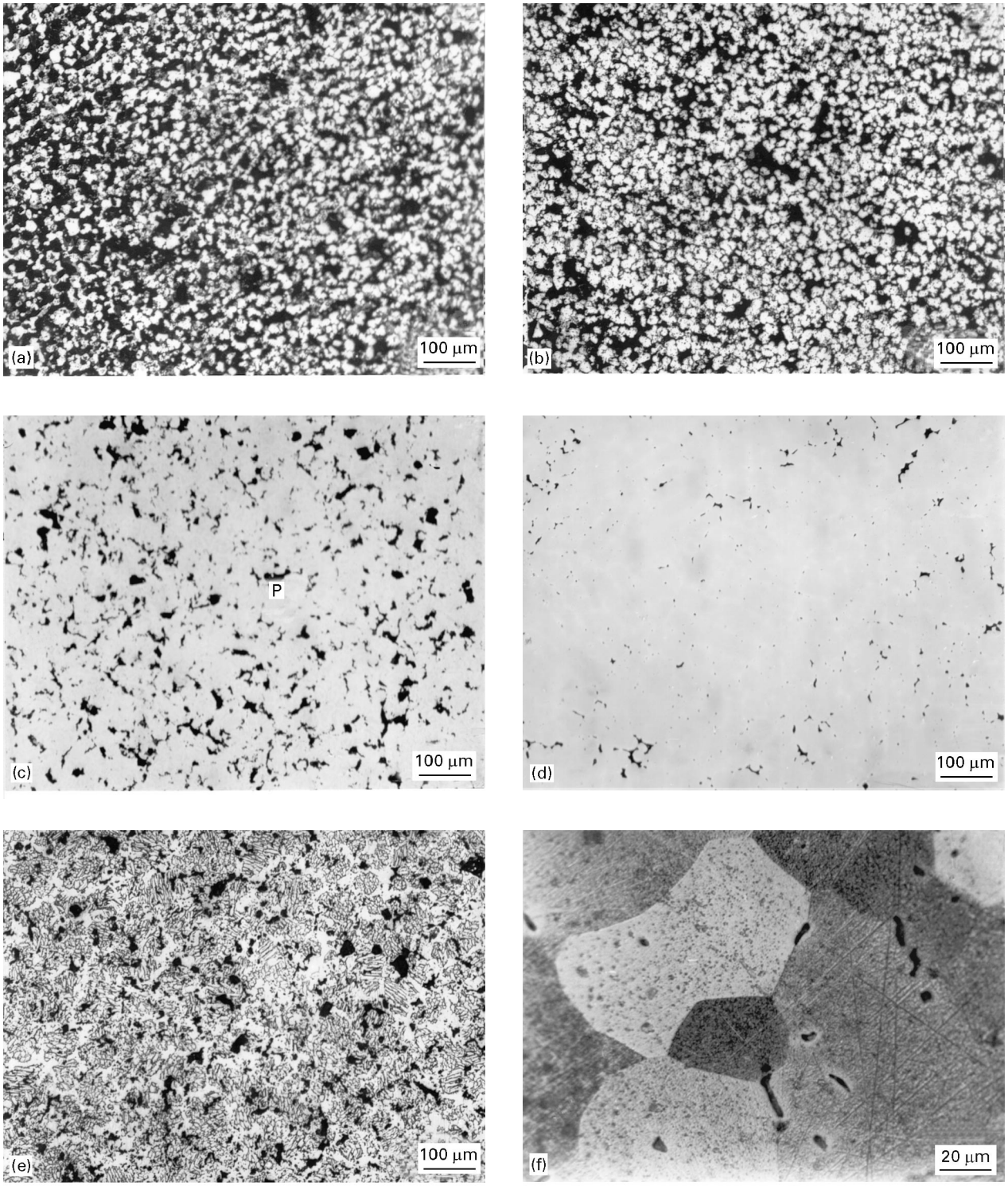

Figure 5 Optical micrographs of the Ni–Al–10Cu–2CeO_2 composites, (a) with 4 wt % Al as-polished, (b) with 12 wt % Al as-polished, (c) with 16 wt % Al as-polished, (d) with 28 wt % Al as-polished, (e) same as (c), but etched with Kalling's reagent, and (f) same as (d), but etched with Kalling's reagent and at a high magnification. Nickel particle size − 300 mesh, compaction pressure 260 MPa, furnace temperature 600 °C.

compositions, single phases corresponding to the Ni_3Al or NiAl compositions in the phase diagrams were detected. For the non-stoichiometric compositions, the primary phases of the composites are Ni, Ni_3Al and NiAl, respectively, depending upon the aluminium content. As can be seen in Fig. 4, in the Ni + Ni_3Al phase region, the amount of Ni_3Al in the composites increases with aluminium content. In the Ni_3Al + NiAl phase region, the amount of the NiAl phase increases with aluminium content, and the amount of the Ni_3Al phase decreases.

Copper is detected in the specimens containing lower aluminium contents from 4–8 wt %, due to the unmelted copper during the synthesis reaction. No apparent copper and copper compounds were detected by X-ray diffraction at higher aluminium contents. Copper has a high solubility in Ni_3Al and NiAl compounds [1], and it might exist either as a solid solution in Ni_3Al or NiAl phases, or in very small amounts in copper compounds, which X-ray diffraction could not detect.

3.3.2. Microstructure

Fig. 5 shows optical micrographs of the composites synthesized by the Ni(2) (<50 μm) powder. The synthesized microstructure of the specimen containing 4 wt % Al is similar to its green compact. The copper particles, red in colour, could be distinguished from the matrix under the optical microscope. The temperature profile in Fig. 2 indicates the exothermic reaction of this composition to be weak. During the synthesis reaction, T_c is higher than the melting point of aluminium (660 °C), but lower than that of nickel (1453 °C) and copper (1083.4 °C), so copper did not melt.

On increasing the aluminium content to more than 16 wt %, the microstructure changes substantially. Fig. 5c shows that most of the small pores originally present have disappeared, but there are still some segments of the original particle boundaries. Arrow P indicates a larger pore between the original powder particles. These large pores might have been previously occupied by aluminium and copper particles, because aluminium and copper melt and flow away along particle or grain boundaries during the reactions, leaving pores behind. The aluminium melt then wets the nickel particles so that the contact surface between nickel and aluminium is enlarged and the reaction between the nickel and aluminium is accelerated. After elemental aluminium is consumed, the liquid phase solidifies, the final microstructure consists of products like Ni_3Al or NiAl and pores.

Fig. 5e shows a eutectic structure in which two phases appear. X-ray diffraction results indicates that the two phases are Ni_3Al and NiAl, and the amount of Ni_3Al is greater than NiAl in these composites. Fig. 5f shows a micrograph of the synthesized NiAl composition in which only a single matrix phase appears. X-ray diffraction results indicate the single matrix phase is NiAl.

Fig. 6 shows scanning electron micrographs of Ni_3Al composite (A-5). The grain size of the Ni_3Al matrix is approximately 15 μm. There are pores around the Ni_3Al grains; the surface of the pores appears powder-like and very rough. X-ray mapping of aluminium and nickel reveals that both elements distribute uniformly inside Ni_3Al grains. However, some porous areas around Ni_3Al grains appear to be aluminium-rich. This indicates that aluminium melts during the synthesis reaction and spreads over the surface of nickel particles with which it reacts. CeO_2 particles are found on the surface of pores, which is illustrated in Fig. 6c. Because CeO_2 has a very high melting point (2600 °C), which is much higher than the combustion temperature, T_c, during the synthesis, CeO_2 particles tend to stay on the pore surface after synthesis has occurred.

The microstructure of the samples containing higher aluminium contents (>20 wt %) shows two different regions; one is a dense area, the other contains voids and large pores. Fig. 6d shows the scanning electron micrograph of the NiAl composition. The cross-section of the composite shows that the final synthesized composite contained some trapped macro-voids. This may be due to the evolution of the gas during the synthesis or the agglomeration of the initial pores during the liquid–liquid reactions. The composite is quite dense and the overall porosity is about 5%–7%. For the stoichiometric NiAl composition, the preliminary SEM results show that CeO_2 tends to segregate to the macro-voids. In the uniform region of the composite, no noticeable CeO_2 is detected by SEM/EDX. This indicates that the CeO_2 has the tendency to segregate to the macro-voids during the liquid–liquid reaction in the NiAl composition. This is similar to what happens in cast metals. The conventional arc melting and the following casting usually

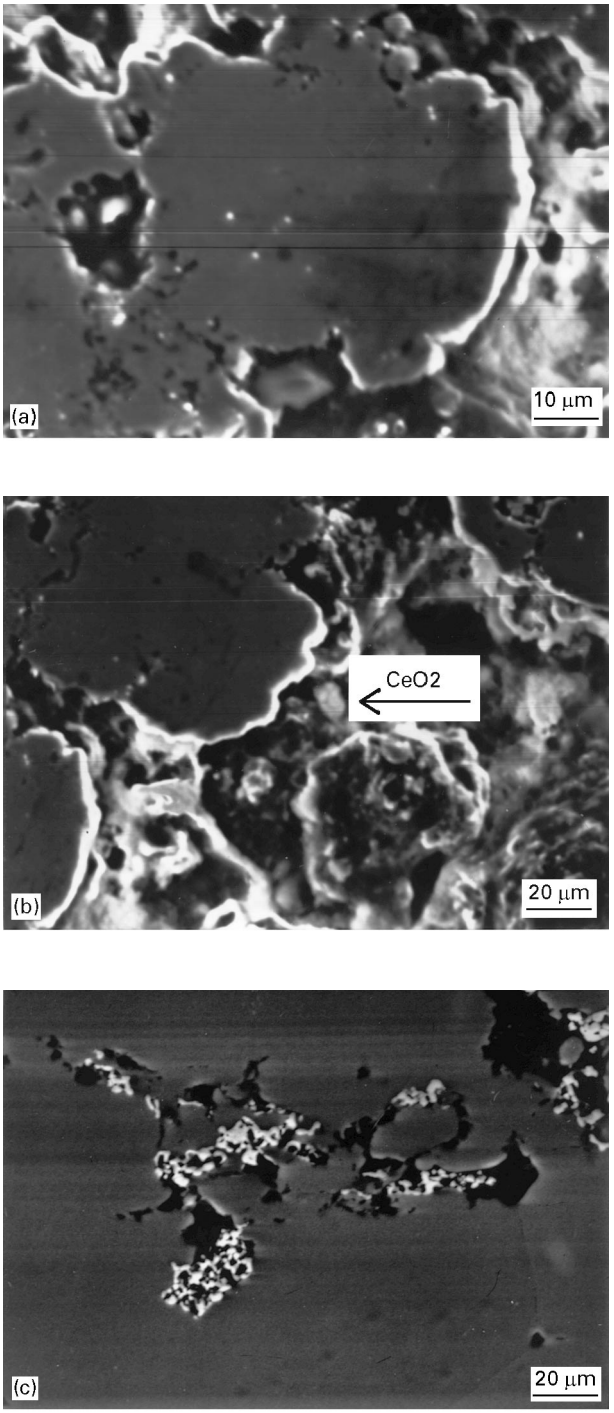

Figure 6 Scanning electron micrographs of Ni_3Al and NiAl composite: (a) secondary electron image of Ni_3Al (A-5); (b) secondary electron image showing a CeO_2 particle in the Ni_3Al (A-5) sample; (c) secondary electron image of NiAl (A-8).

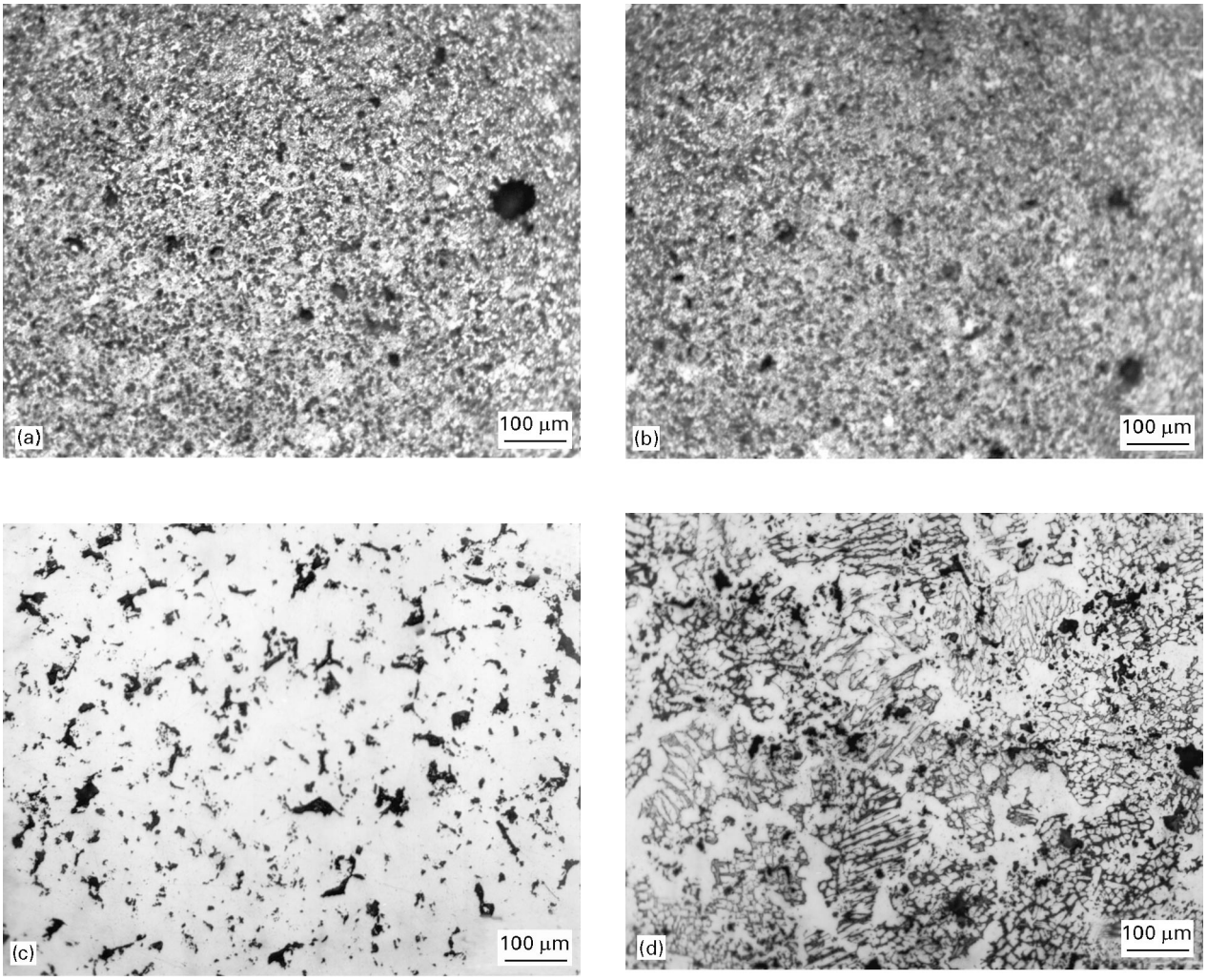

Figure 7 Optical micrographs of Ni–Al–10Cu–2CeO_2 composites synthesized from fine nickel powder (~3 μm): (a) 4 wt % Al, as-polished; (b) 12 wt % Al, as-polished; (c) 16 wt % Al, as-polished; (d) 16 wt % Al, etched with Kalling's reagent. Compaction pressure 215 MPa, furnace temperature 600 °C.

exhibit difficulties in fabricating particulate-reinforced alloys due to the agglomeration of the particulate.

Figs 7 and 8 illustrate the microstructure of the composites synthesized using Ni(3) (~3 μm) and Ni(1) (<149 μm) powders, respectively. The microstructure reflects the fact that the fine nickel particle size, Ni(3), results in a small grain size, small pore size and uniform pore distribution, but it also causes slightly higher final porosity. The final porosity of the composites is shown in Fig. 9.

3.4. Mechanical properties

3.4.1. Hardness

In Fig. 10 the variations in Vickers hardness of Ni–Al–10Cu–2CeO_2 composites with aluminium content are shown. The hardness initially increases slightly with aluminium up to 12 wt %, and then increases remarkably with aluminium content. The increase in hardness can be divided into two ranges depending on the aluminium content. For aluminium contents ranging from 4–12 wt %, the phases of the composite matrix are mainly nickel and/or Ni_3Al. An increase in the hardness is primarily due to a decrease in porosity and an increase in Ni_3Al content. For aluminium contents ranging from 12–28 wt %, the increase in hardness is mainly attributed to the dramatic decrease in the final porosity of the composites.

3.4.2. Flexural strength

The results from a total of five fracture tests obtained from four different compositions show variation in failure strength. Simple Weibull statistics [25] are used to analyse the flexural strength data. Fig. 11 shows a simple Weibull strength–probability curve for the Ni–6Al–10Cu–2CeO_2 composites. The characteristic strength of the tested specimen is the stress for which the vertical axis is 63.2%. The simple Weibull statistics analysis gives the characteristic flexural strength of 66 MPa for this composite.

Fig. 12 shows the dependence of flexural strength and the modulus of elasticity on the aluminium content of the composites. The flexural strength and the modulus increases with the aluminium content. Fig. 13 shows the flexural yield strength and the modulus of elasticity versus final porosity in the Ni–Al–10Cu–CeO_2 composites. Both flexural strength and the modulus decrease significantly with increasing porosity. The increase in the porosity

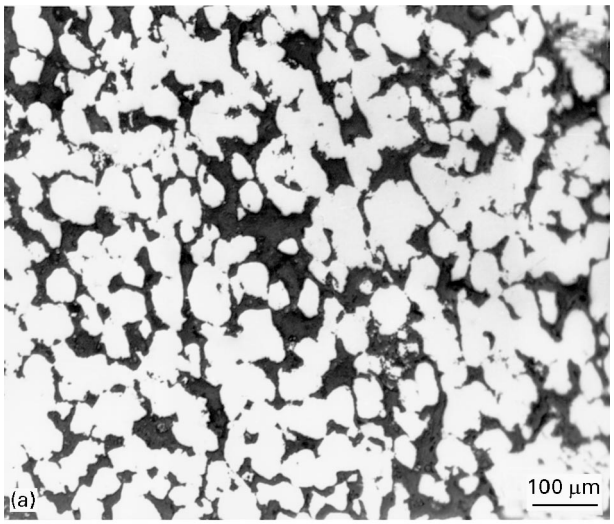

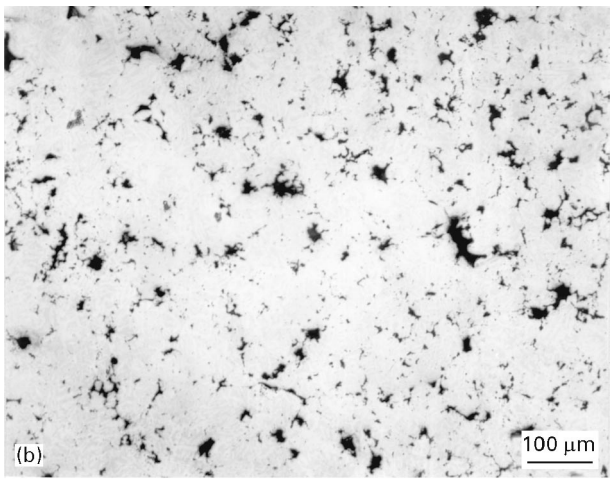

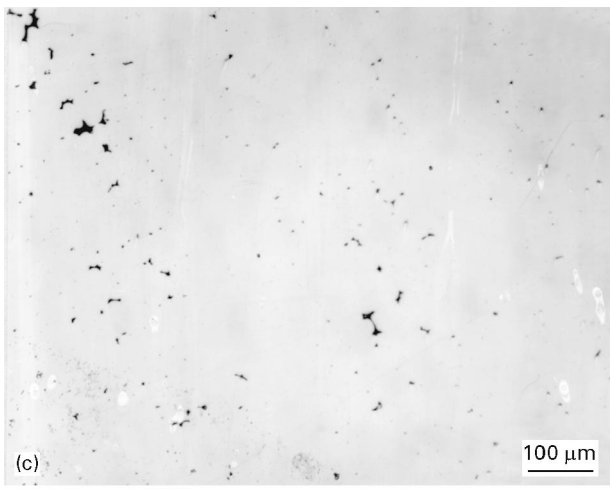

Figure 8 Optical micrographs of Ni–Al–10Cu–2CeO_2 composites synthesized by coarser nickel powder (<149 μm): (a) 12 wt % Al, as polished; (b) 16 wt % Al, as-polished; (c) 28 wt % Al, as-polished. Compacting pressure 215 MPa, furnace temperature 600 °C.

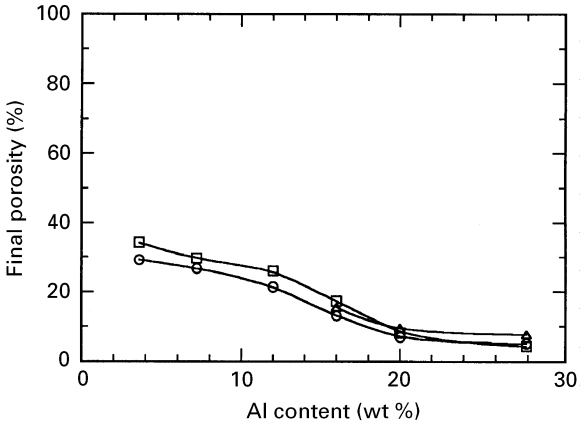

Figure 9 Final porosity versus aluminium content for Ni (○) < 149 μm, (□) <50 μm and (△) ~3 μm. Processing conditions: compaction pressure 215 MPa, furnace temperature 600 °C.

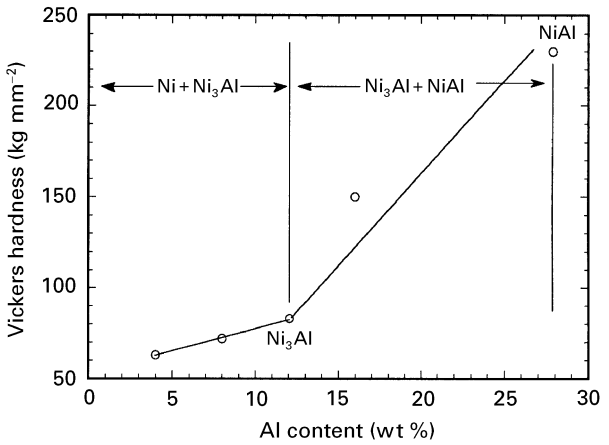

Figure 10 Vickers hardness as a function of aluminium content in the Ni–Al–10Cu–2CeO_2 composites. Nickel particle size − 100 mesh, compaction pressure 215 MPa, furnace temperature 800 °C.

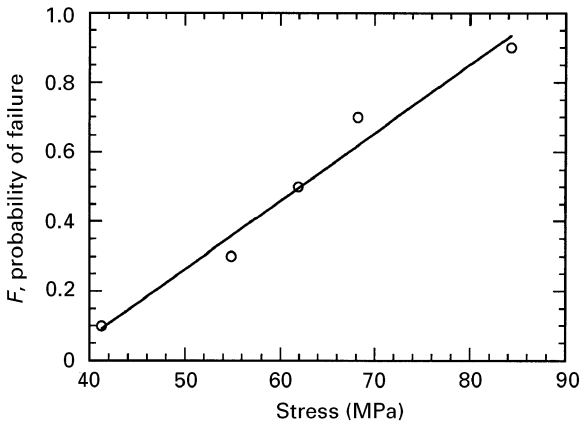

Figure 11 Weibull strength–probability curve for the Ni–6Al–10Cu–2CeO_2 composites. Nickel particle size − 100 mesh, compaction pressure 215 MPa, furnace temperature 800 °C.

decreases the cross-sectional area on which the load is applied. The pores also act as stress concentrators and as an initial source of cracks.

Fig. 14 illustrates the fracture surface of the Ni_3Al–10Cu–2CeO_2 composite. The fracture morphology of the specimen shows two different fracture patterns depending on the aluminium content. At lower aluminium contents (4–8 wt % Al), the fracture surfaces are powder-like and quite rough. The pores connect across the fracture surface. The surface of the pores and the fracture surface of the composite matrix are very similar. Fracture occurs at the grain

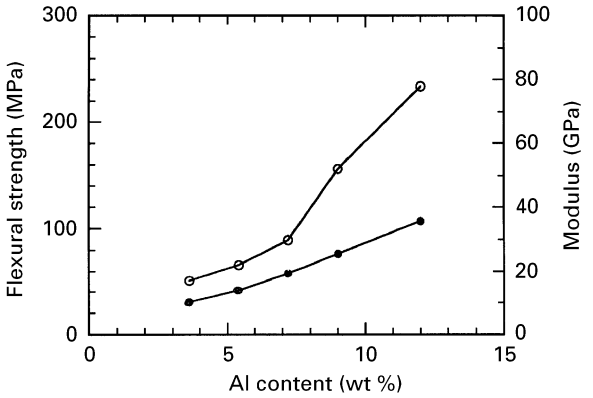

Figure 12 (○) Flexural yield strength and (●) the modulus of elasticity of Ni–Al–10Cu–2CeO_2 composites as a function of aluminium content. Nickel particle size − 100 mesh, compaction pressure 215 MPa, furnace temperature 800 °C.

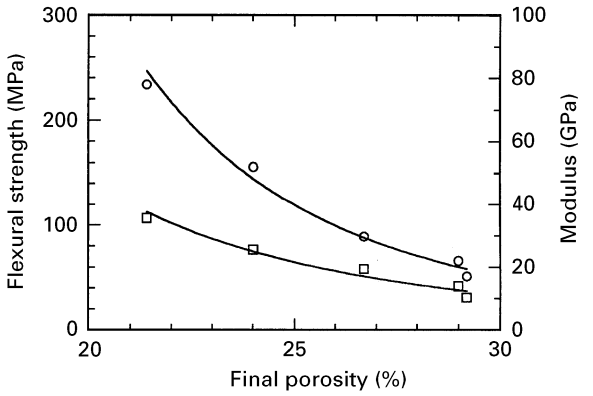

Figure 13 (○) Flexural yield strength and (□) the modulus of elasticity versus final porosity in Ni–Al–10Cu–2CeO_2 composites. Nickel particle size − 100 mesh, compaction pressure 215 MPa, furnace temperature 800 °C.

boundaries of the matrix and propagates across the surface by micro-void coalescence.

For Ni_3Al stoichiometric composition, the fracture surface shows two types of features, one is a powder-like pattern which is quite similar to that found at lower aluminium content. Another type of fracture feature, which is distinct from the powder-like pattern, appears as a relatively flat and smooth surface. This is a typical brittle fracture surface of Ni_3Al phase. This indicates that intergranular fracture occurs in the Ni_3Al matrix. The flexural test indicates that the Ni_3Al stoichiometric composition shows the highest flexural strength among the tested compositions. In addition to the decrease of the porosity in the composites with increasing aluminium content, the increase in the strength of the grain boundaries of Ni_3Al also contributes to the increase in the flexural strength of the Ni–Al–Cu–2CeO_2 composites.

4. Conclusions

The processing and properties of micropyretically synthesized Ni–Al–Cu–CeO_2 intermetallic composites were studied. The effect of processing parameters such as chemical composition, heating rate, particle size and compaction pressure on the response processing parameters, such as ignition and combustion temperature, phases of composites, microstructure and mechanical properties, were studied in detail. In the Ni–Al–Cu– CeO_2 system with aluminium contents ranging from 4–12 wt %, the results shows that T_c increases with increasing aluminium content, while T_i decreases slightly with increasing aluminium content. T_c increases with heating rate, while no appreciable change in T_i with heating rate is found.

The four-point bending test indicates that the flexural strength and the modulus increase with increasing aluminium content. The fracture morphology of the composites shows two different patterns depending on the aluminium content. At lower aluminium contents, the fracture surfaces appear powder-like and are quite rough. The surfaces of the pores and the matrix in the composites are very similar. At Ni_3Al stoichiometric composition in which the aluminium content is 12 wt %, the fracture surface shows two types of features. One is powder-like, which is quite similar to that found at lower aluminium content; the other is a relatively flat and smooth surface, which characterizes the typical brittle intergranular fracture of the Ni_3Al composite.

References

1. N. S. STOLOFF, *Int. Mater. Rev.* **34** (1989) 153.
2. P. C. BRENNAN and W. H. KAO, *Mater. Sci. Eng.* **A153**, (1992) 635.

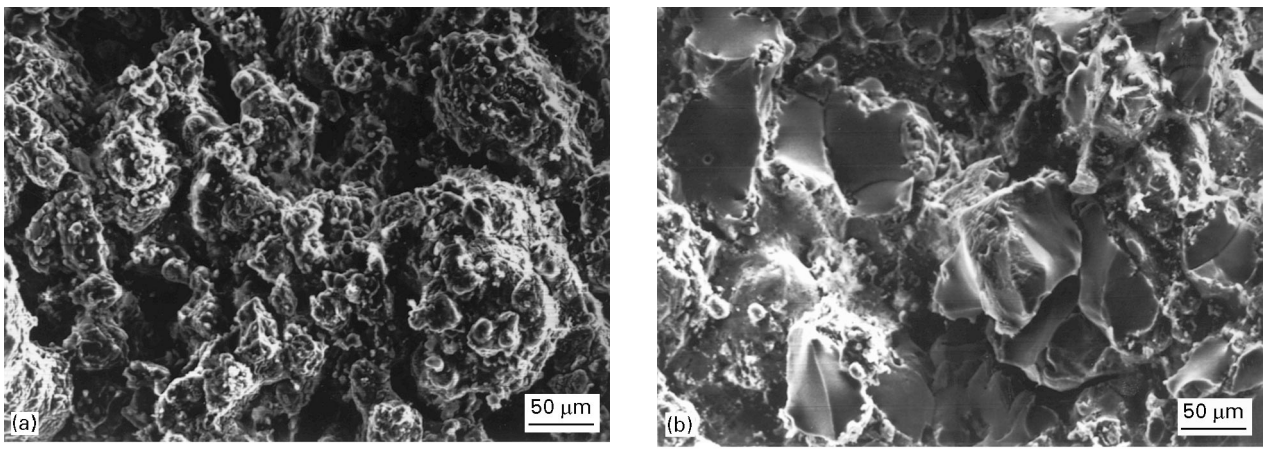

Figure 14 Fracture surface of the Ni–Al–10Cu–2CeO_2 composites: (a) 8 wt % Al, (b) 12 wt % Al.

3. G. E. FUCHS, *J. Mater. Res.* **5** (1990) 1649.
4. P. C. BRENNAN, W. H. KAO, S. M. JENG and J.-M. YANG, in "Materials Research Society Symposium Proceedings", Vol. 194, edited by D. L. Anton (MRS, Pittsburgh, 1990) p. 169.
5. C. G. McKAMEY and E. H. LEE, *ibid*., p. 163.
6. D. E. ALMAN and N. S. STOLOFF, in "Materials Research Society Symposium Proceedings", Vol. 213, edited by D. B. Mirade and D. L. Anton (MRS, Pittsburgh, 1991) p. 989.
7. I. A. IBRAHIM, F. A. MOHAMED and E. J. LAVERNIA, *J. Mater. Sci.* **26** (1991) 1137.
8. H. P. LI, S. B. BHADURI and J. A. SEKHAR, *Metall. Trans.* **23A** (1992) 251.
9. *Idem*, in "Processing and Fabrication of Advanced Materials for High Temperature Application", edited by V. A. Ravi and T. S. Srivatsan (TMS, Warrendale, PA, 1992) p. 45.
10. H. P. LI and J. A. SEKHAR, in "Advanced Synthesis of Engineered Structural Materials", edited by J. J. Moore, E. J. Lavernia and F. H. Froes (ASM International Materials Park, OH, 1993) p. 25.
11. *Idem*, *J. Mater. Res.* **8** (1993) 2515.
12. *Idem*, *Mater. Sci. Eng.* **A160** (1993) 221.
13. Z. A. MUNIR and U. ANSELMI-TAMBURINI, *Mater. Sci. Rep.* **3** (1989) 1993.
14. D. E. ALMAN, in "Advances in Powder and Particulate Materials – 1992", Vol. 9, edited by J. M. Capus and R. M. German (MPIF and APMI, Princeton, NJ, 1993) p. 441.
15. K. A. PHILPOT, Z. A. MUNIR and J. B. HOLT, *J. Mater. Sci.* **22** (1987) 159.
16. C. NISHIMURA and C. T. LIU, *Acta Metall. Mater.* **41** (1993) 113.
17. D. M. SIMS, A. BOSE and R. M. GERMAN, *Prog. Powder Metall.* **43** (1987) 575.
18. A. BOSE, B. H. RABIN and R. M. GERMAN, *Powder Metall. Int.* **20** (1988) 25.
19. A. BOSE, B. MOORE, R. M. GERMAN and N. S. STOLOFF, *J. Metals* **9** (1988) 14.
20. J. P. LEBRAT, A. VARMA and A. E. MILLER, *Metall. Trans.* **23A** (1992) 69.
21. K. S. HWANG and Y. C. LU, *Powder Metall. Int.* **24** (1992) 279.
22. K. E. MOHAMED, D. STOVER and H. P. BUCHDREMER, in "Advances in Powder and Particulate Materials – 1993", Vol 9, edited by J. M. Capus and R. M. German (MPIF and APMI, Princeton, NJ, 1993) p. 423.
23. H. ZHANG, J. A. SEKHAR, J. J. DURUZ and V. de NORA, *J. Mater. Res*., submitted.
24. G. PETZOW and G. EFFENBEG, "Ternary Alloys: A Comprehensive Compendium of Evaluated Constitutional Data and Phase Diagrams", Vol. 4 (VCH, Verlagsgesellschaft, Weinhelm, Germany and VCH, New York, NY, 1988).
25. G. D. QUINN, in "Engineered Materials Handbook", Vol. 4, "Ceramic and Glasses" edited by S. J. Schneider, Jnr. (ASM International, Materials Park, OH, 1991) p. 586.

Received 19 January
and accepted 31 July 1996